Computer simulation of the a-Si:H p–i–n solar cell performance sensitivity to the free carrier's mobilities, the capture cross sections and the density of gap states

2006 J. Phys.: Condens. Matter 18 9435

(http://iopscience.iop.org/0953-8984/18/41/010)

INSTITUTE OF PHYSICS PUBLISHING JOURNAL OF PHYSICS: CONDENSED MATTER

J. Phys.: Condens. Matter **18** (2006) 9435–9446 doi:10.1088/0953-8984/18/41/010

Computer simulation of the a-Si:H p–i–n solar cell performance sensitivity to the free carrier's mobilities, the capture cross sections and the density of gap states

A F Meftah[1,3], **A M Meftah**[1] **and A Belghachi**[2]

[1] Faculté des Sciences, Laboratoire des Matériaux Semi-conducteurs et Métalliques, Université Mohammed Khider, BP 145, Biskra 07000, Algeria
[2] Laboratory of Semiconductor Devices Physics, Physics Department, University of Béchar, PO Box 417, Béchar 08000, Algeria

E-mail: af_mef@yahoo.fr

Received 6 June 2006, in final form 5 September 2006
Published 29 September 2006
Online at stacks.iop.org/JPhysCM/18/9435

Abstract

This paper deals with the effects of some material properties on the J–V characteristic of hydrogenated amorphous silicon (a-Si:H)-based p–i–n solar cell. The factors considered are the free carrier's mobilities, the capture cross sections of the gap states and the bulk density of states (i-layer DOS). Accurate investigation of the cell photo-parameters' sensitivity to these factors is carried out using a simulation program, previously developed by our group. The model is based on a complete set of Poisson and carrier continuity equations taking into account the defect pool model for the a-Si:H gap density of states. Ours results reveal the important role of the hole mobility when it takes low values, as given frequently in the literature, on the recombination rate at interface regions as well as in the bulk. This considerably affects the short-circuit current density (J_{sc}), the open-circuit voltage (V_{oc}), the fill factor (FF) and the conversion efficiency (η). Moreover, by changing separately the capture cross sections of the band's tails and those of dangling bonds we found more precisely that J_{sc}, V_{oc}, and η are more sensitive to the interface recombination while the FF seems to depend more on the bulk recombination. Ultimately, when the i-layer DOS is higher than 10^{16} cm^{-3}, the recombination rate, which was first limited by the valence band tail's states, becomes limited by the dangling bond's states. Then, any further increase significantly deteriorates the solar cell performance.

1. Introduction

Expectations of an early reestablishment in the terrestrial environment's state depend strongly on the use of environmentally friendly energy sources, like solar cells. One of the promoter

[3] Author to whom any correspondence should be addressed.

materials employed, with cheap cost, in the fabrication of such alternatives is hydrogenated amorphous silicon (a-Si:H). This type of material has higher absorption coefficient in the visible range than monocrystalline Si, and can be deposited on any substrate in large areas at a temperature less than 300 °C [1]. Many structures of a-Si:H-based solar cells (single or multijunctions) have been produced with the aim to enhance their conversion efficiency and to reduce their sensitivity to the light soaking effect. In our study, we try to shed light on a number of factors that limit cell performance in the single p–i–n junction. This is done through a computer simulation model [2, 3], which presents a good tool for studying the electrical transport properties within the device, and for understanding the role of several parameters related either to the material properties (gap mobilities, density of states, etc) or to the cell structure (doping, layer's thicknesses, etc). In this work, we have particularly focused on the effects of the free carrier's mobilities, the capture cross sections of both tails and dangling bond states, and the i-layer density of states (DOS), on the output photo-parameters of the proposed solar cell, i.e., the short-circuit current density (J_{sc}), the open-circuit voltage (V_{oc}), the fill factor (FF), and the conversion efficiency (η).

2. Numerical modelling

The a-Si:H p–i–n solar cell is treated as a one-dimensional device. Our simulation program developed previously [2, 3], simultaneously solves the Poisson equation and the two continuity equations of free carriers [4, 5] under steady state conditions, using the coupled method of Newton. This is performed by taking into account the usual model of the a-Si:H gap density of states, consisting of the band tails and dangling bond states [6, 7]. Further, the density of states is calculated according to the defect pool model of Powell and Deane [13] which differs form previously proposed numerical models that adopt Gaussian distributions to describe the dangling bond density of states [8–12]. Moreover, a spatial distribution of this density along the device, as a consequence of the variation of the Fermi-level position within the energy gap is considered [2, 3]. In addition, we have assumed a thin p/i interface layer with a high density of dangling bond states [8, 9, 14, 3]. The presence of such a region has been revealed by many experimental measurements [15–18], and can be attributed to the specific characteristics of the growth process.

The p–i–n diode considered operates under global standard solar spectrum (AM1.5) illumination. Both glass/transparent conductive oxide (TCO) substrate transmittance and n/metal contact reflectivity are taken into account, while the TCO/p contact reflectivity is neglected.

3. Results and discussion

The simulation parameters used to generate the output photo-parameters of the solar cell are indicated in table 1. We note that the p/i interface dangling bond states have capture cross sections identical to those supposed for the dangling bond states in the bulk. The choice of the capture cross section's values of dangling bonds (σ_{cd} of the charged states and σ_{nd} of the neutral ones) is related to the calculation of the dark reverse current density, J. The latter also depends on the mobility gap energy, E_g, the density of states (DOS) [9] and the p/i interface defect density, N_{pi} [9, 3]. Then, for a given E_g, DOS and N_{pi}, which are in this case 1.8 eV, 5×10^{15} cm^{-3} and 3×10^{18} cm^{-3}, respectively, σ_{cd} and σ_{nd} have to be adjusted so that J reaches the experimental measurement range, that is [10^{-12}–10^{-10} A cm^{-2}] [10]. As shown in figure 1(a), this condition has been fulfilled when $\sigma_{cd}/\sigma_{nd} \geqslant 5 \times 10^{-15}/5 \times 10^{-16}$ cm^2.

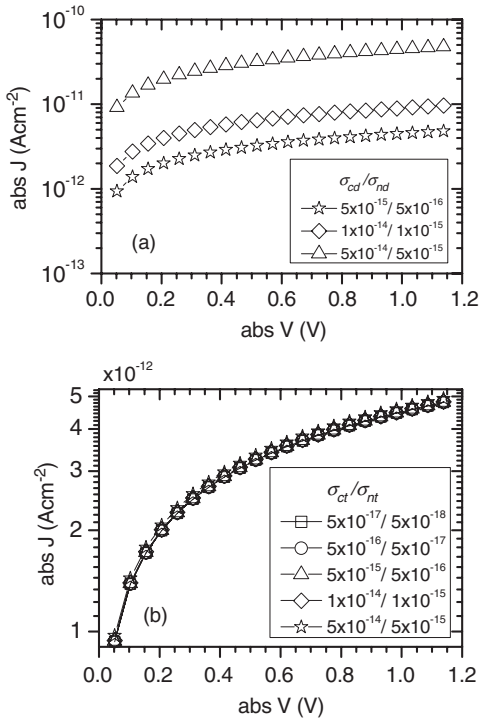

Figure 1. Dark reverse current density when (a) $\sigma_{ct}/\sigma_{nt} = 5 \times 10^{-15}$ cm^2/5×10^{-16} cm^2, and (b) $\sigma_{cd}/\sigma_{nd} = 5 \times 10^{-15}$ cm^2/5×10^{-16} cm^2.

Table 1. Input parameters for the a-Si:H p–i–n solar cell.

p-layer thickness (nm)	10
p/i-interface thickness (nm)	3
i-layer thickness (nm)	477
n-layer thickness (nm)	10
Mobility gap, E_g (eV)	1.8
Activation energy in the p layer, E_{fp} (eV)	0.42
Activation energy in the n layer, E_{fn} (eV)	0.22
Effective density in the valence and conduction bands, N_c, N_v (cm^{-3})	2×10^{20}
Characteristic energy of the valence band tail (eV)	0.043
Characteristic energy of the conduction band tail (eV)	0.025
i-layer DOS (cm^{-3})	5×10^{15}
p/i DOS, N_{pi} (cm^{-3})	3×10^{18}
Free electron's mobility, μ_n (cm^2 V^{-1} s^{-1})	20
Free hole's mobility, μ_p (cm^2 V^{-1} s^{-1})	2
Capture cross section of charged tail's states, σ_{ct} (cm^2)	5×10^{-15}
Capture cross section of neutral tail's states, σ_{nt} (cm^2)	5×10^{-16}
Capture cross section of charged dangling bond's states, σ_{cd} (cm^2)	5×10^{-15}
Capture cross section of neutral dangling bond's states, σ_{nd} (cm^2)	5×10^{-16}
Glass/TCO substrate transmittance	0.9 [8]
n/metal contact reflectivity	0.9 [8]

However, the increase of the capture cross sections of charged (σ_{ct}) and neutral (σ_{nt}) band tails does not affect J at all, as shown in figure 1(b). We will see later that this is not the case for the output photo-parameters of the solar cell.

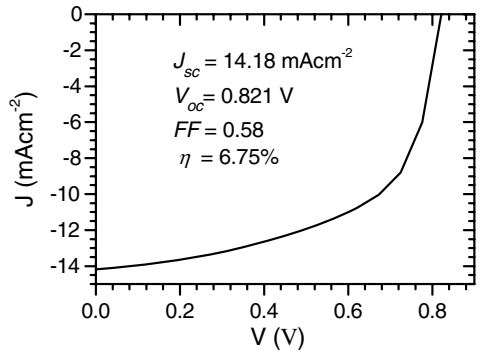

Figure 2. J–V characteristic of the a-Si:H p–i–n solar cell with a whole thickness of 0.5 μm.

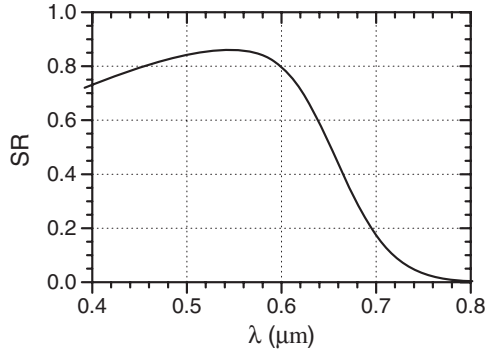

Figure 3. Spectral response of the a-Si:H p–i–n solar cell with a whole thickness of 0.5 μm at the short-circuit condition.

Figures 2 and 3 show the calculated J–V characteristic and the spectral response, SR (external quantum efficiency), of the proposed cell structure. The obtained output photo-parameters, $J_{sc} = 14.18$ mA cm^{-2}, $V_{oc} = 0.82$ V, FF $= 0.58$ and $\eta = 6.75\%$, are close to the ones measured generally in conventional single a-Si:H p–i–n solar cells [1, 19, 20]. The external quantum efficiency is 0.73 at 0.4 μm and reaches a maximum value, about 0.85, between 0.52 and 0.56 μm; afterwards, it decreases strongly at long wavelengths. This result is in fair agreement with the experimental external quantum efficiency curve given in [11] for a p–i–n structure solar cell with an i-layer thickness of 0.450 μm.

To be more precise in the model corroboration checking, we try to simulate the experimental output photo-parameters of the a-Si:H p–i–n solar cell indicated in [20]. The thicknesses of the p, i and n layers are fixed, respectively equal to 16, 640 and 40 nm, where the activation energies at the p and n layers are, respectively, $E_{fp} = 0.19$ eV and $E_{fn} = 0.1$ eV, similarly to [20]. The input parameter values used to obtain the best agreement with the experimental measurements of [20] are $\mu_n = 20$ cm^2 V^{-1} s^{-1}, $\mu_p = 4$ cm^2 V^{-1} s^{-1}, $N_{pi} = 3 \times 10^{19}$ cm^{-3}, $\sigma_{ct} = 1 \times 10^{-16}$ cm^2 and $\sigma_{nt} = 1 \times 10^{-17}$ cm^2, while the remaining parameters are the same as the ones indicated in table 1. The results obtained are summarized in table 2, from which we find that the agreement is satisfactory.

3.1. Effect of the free carrier's mobilities on the cell output photo-parameters

It has been found on the basis of field-effect studies that $\mu_n = 20$ cm^2 V^{-1} s^{-1} [21], and an analysis of both single and double injection into amorphous silicon alloys has indicated

Table 2. Comparison between model and experimental data from [18].

	J_{sc} (mA cm^{-2})	V_{oc} (V)	FF	η (%)
Model	13.63	0.835	0.643	7.32
Experimental [20]	14.10 ± 0.43	0.8 ± 0.02	0.62 ± 0.021	7 ± 0.28

Table 3. Output photo-parameters of the solar cell obtained by varying μ_n and μ_p separately.

μ_n/μ_p	J_{sc} (mA cm^{-2})	V_{oc} (V)	FF	η (%)	μ_n/μ_p	J_{sc} (mA cm^{-2})	V_{oc} (V)	FF	η (%)
10/2	13.996	0.838	0.565	6.61	20/2	14.187	0.821	0.58	6.75
20/2	14.187	0.821	0.58	6.75	20/4	14.455	0.826	0.618	7.387
25/2	14.214	0.812	0.587	6.8	20/6	14.514	0.83	0.644	7.763

Table 4. Output photo-parameters calculated for the solar cell when both μ_n and μ_p are changed but with preserving the μ_n/μ_p ratio constant.

$\mu_n/\mu_p = 10$	J_{sc} (mA cm^{-2})	V_{oc} (V)	FF	η (%)	$\mu_n/\mu_p = 5$	J_{sc} (mA cm^{-2})	V_{oc} (V)	FF	η (%)
10/1	13.46	0.834	0.535	6.01	10/2	13.996	0.838	0.565	6.61
20/2	14.187	0.821	0.58	6.75	20/4	14.455	0.826	0.618	7.387
25/2.5	14.345	0.815	0.596	6.974	25/5	14.546	0.82	0.638	7.615

Table 5. Free carrier's mobilities effects in terms of percentages.

	ΔJ_{sc} (%)	ΔFF (%)	$\Delta\eta$ (%)	ΔV_{oc} (%)
μ_n = 10–25 (cm^2 V^{-1} s^{-1}) μ_p = 2 (cm^2 V^{-1} s^{-1})	+1.55	+3.89	+2.87	−3.2
μ_n = 20 (cm^2 V^{-1} s^{-1}) μ_p = 2–6 (cm^2 V^{-1} s^{-1})	+2.3	+11.03	+15.2	+1.096
μ_n = 10–25 (cm^2 V^{-1} s^{-1}) μ_n/μ_p = 10	+6.57	+11.4	+16.04	−2.27
μ_n = 10–25 (cm^2 V^{-1} s^{-1}) μ_n/μ_p = 5	+3.92	+12.92	+15.2	−2.14

that $\mu_p = 4$ cm^2 V^{-1} s^{-1} [21]. Generally, in normal a-Si:H material μ_n is greater than 10 cm^2 V^{-1} s^{-1} and μ_p is less than 6 cm^2 V^{-1} s^{-1} [12]. The variation of μ_n and μ_p is useful in determining the limitations to device performance and in understanding the physics controlling these limitations. To investigate in more detail the effect of the free carrier's mobilities on the output photo-parameters of the solar cell, two cases have been considered. In the first, one of the free carrier's mobilities has been fixed (for example μ_n) while the other (μ_p) was varied, and vice versa. However, in the second case both μ_n and μ_p have been varied while preserving the μ_n/μ_p ratio constant. The results obtained for these two cases are summarized in tables 3 and 4, respectively. Table 5 assembles these effects in terms of the maximum difference (percentages). From the latter, we can observe that J_{sc}, FF and η increase when μ_n increases, and this increase is more significant when μ_p increases too. Contrarily, V_{oc} decreases as μ_n increases, and this is less noticeable if μ_p increases. In addition, the values $\mu_n = 25$ cm^2 V^{-1} s^{-1} and $\mu_p = 6$ cm^2 V^{-1} s^{-1} [12] seem to provide the better output photo-parameters for the proposed solar cell structure (see table 6).

Table 6. Values of μ_n and μ_p that give better conversion efficiency for the solar cell.

μ_n/μ_p	J_{sc} (mA cm^{-2})	V_{oc} (V)	FF	η (%)
25/6	14.568	0.822	0.65	7.784

The results obtained clearly show that μ_p influences the solar cell performance more than μ_n. This owes its origin to the low values of μ_p, which implies the availability of minority carriers that limit recombination [12]. Then any increase in μ_p, provided that it remains low, has more influence on the output parameters of the solar cell. This observation has been pointed out by Chatterjee [12], who found that there is practically no sensitivity to μ_p for $\mu_p > 6$ cm^2 V^{-1} s^{-1} and that only when μ_p becomes less than 6 cm^2 V^{-1} s^{-1} do the solar cell output parameters deteriorate with decreasing μ_p. The crucial role of the low μ_p in the recombination process has been tested by tracing the recombination rate profile over the device for the different cases above (see figures 4(a)–(f)). Indeed, we can see from these figures that the recombination rate profile changes appreciably over the device when μ_p increases from 2 to 5 or 6 cm^2 V^{-1} s^{-1}, except at the p/i interface region. Even though it is μ_p that plays the predominant role in recombination, we cannot totally ignore that μ_n has also some influence when it drops to 10 cm^2 V^{-1} s^{-1}, except at the i/n interface region (figure 4(a)). Moreover, this is apparent only at 0 V, while at 0.5 V the sensitivity to μ_n is almost insignificant (see figure 4(b)). The insensitivity of the recombination rate to μ_p at the p/i interface region or to μ_n at the i/n interface can be explained as follows: when μ_n increases, the expulsion of the free electrons by the electrical field from the region where they are the minority carriers (at the p/i interface) is favoured. Then, a decrease of the recombination rate in this region, owing to the np product reduction, is expected, although in this region the high recombination rate is due mainly to the p/i DOS. However, at the i/n interface where the free electrons are the majority carriers, the increase of μ_n does not affect the recombination rate at all. The same explanation holds for free holes as μ_p increases. Then, if both μ_n and μ_p are changed, the recombination rate at the p/i and i/n interface regions will also change, which is shown in figures 4(e), (f).

The expulsion of one type of free carrier (e.g. electrons), supported by the increase of their mobility, from the interface region, where they form the minority, towards the bulk reduces both their capture by the oppositely charged states and their recombination with the majority carriers. Since near the interface region the recombination is due mainly to the high defect density, a decrease in the proportion of the charged states neutralized by the minority carrier capture is expected when their mobility increases. This means that the increase of the minority carrier mobility implies that more of the charged states are not neutralized in the region considered. However, the expulsion of the considered free carriers from the interface region, where they form the majority, toward the contact implies the decrease of the dominant charge in this region (which has the same sign of the majority carriers). Thus, we expect that the electrical field increases on increasing the carrier mobility in the first region (where the considered free carriers are the minority) since there is an increase in the dominant charge, while it decreases in the second region (where the considered free carriers are the majority). This is clearly shown in figures 5(a), (b): near the p/i interface, where the dominant charge is positive and the minority carriers expulsed are the electrons, there is a slight increase of the electrical field as μ_n increases, while near the i/n interface it decreases slightly, because of the reduction of the dominant charge (which is negative in this region). The same remark can be made from figures 5(c), (d) for holes.

Moreover, a very interesting result is observed in figures 5(e), (f). When the μ_n/μ_p ratio is kept constant, the electrical field profile hardly changes. This can be attributed to the fact that the same μ_n/μ_p ratio implies the availability of the same charge density (a null variation rate).

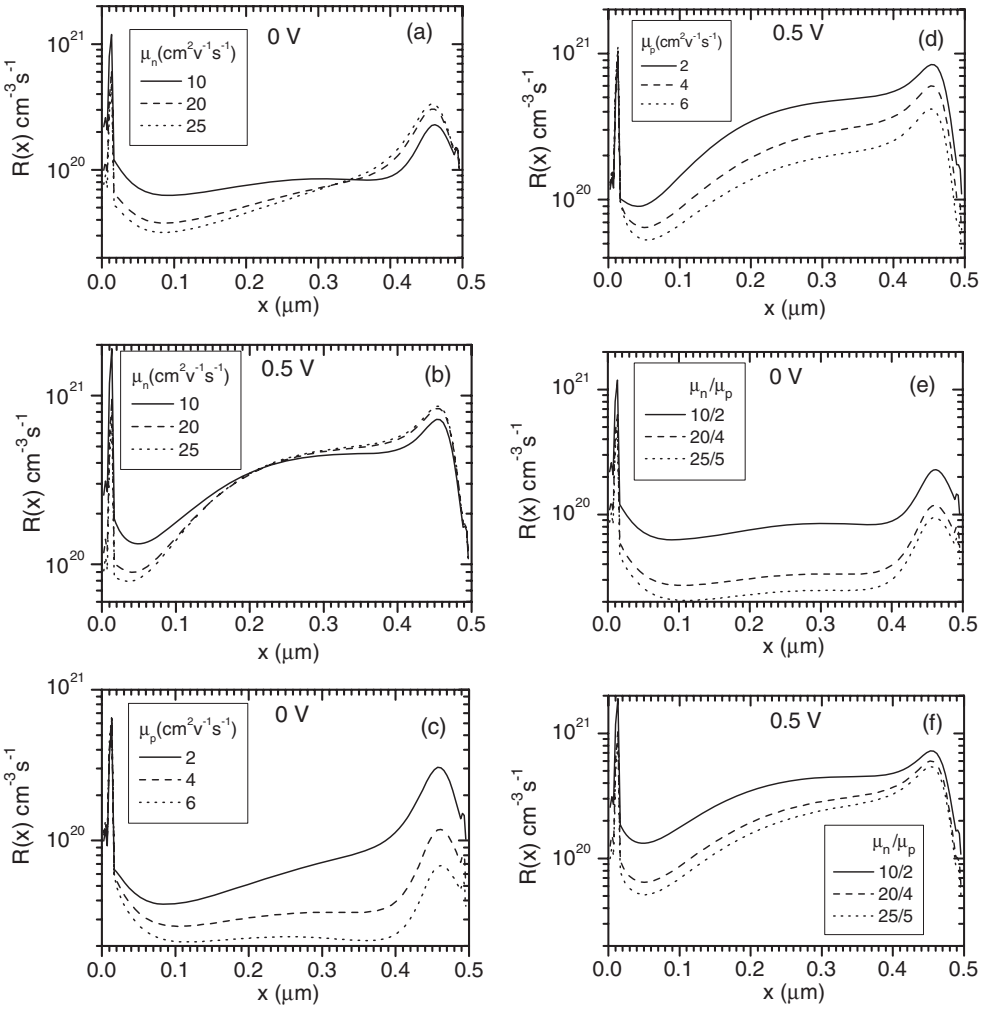

Figure 4. Recombination rate versus position (a) at 0 V when μ_p is fixed to 2 cm^2 V^{-1} s^{-1}, (b) at 0.5 V when μ_p is fixed to 2 cm^2 V^{-1} s^{-1}, (c) at 0 V when μ_n is fixed to 20 cm^2 V^{-1} s^{-1}, (d) at 0.5 V when μ_n is fixed to 20 cm^2 V^{-1} s^{-1}, (e) at 0 V when the μ_n/μ_p ratio is fixed to 5, and (f) at 0.5 V when the μ_n/μ_p ratio is fixed to 5.

3.2. Effect of the capture cross section on the cell output photo-parameters

Tables 7–9 recapitulate the effect of the capture cross sections on the output photo-parameters of the proposed cell structure. For these calculations, the carrier mobilities have been fixed to $\mu_n = 25$ cm^2 V^{-1} s^{-1} and $\mu_p = 6$ cm^2 V^{-1} s^{-1}. From tables 7 and 8, we can see that the increase of σ_{cd}/σ_{nd} to 5×10^{-14} cm^2/5×10^{-15} cm^2 reduces more significantly the output photo-parameters of the solar cell than that of σ_{ct}/σ_{nt}, except for FF. This is certainly due to the high recombination rate near the p/i and i/n interfaces, resulting mainly from the highest DOS. As a consequence, the recombination rate in these regions is more sensitive to the increase of σ_{cd}/σ_{nd} than that of σ_{ct}/σ_{nt}, contrarily to the bulk recombination, as shown in figures 6(a), (b).

On the other hand, the decrease of σ_{ct}/σ_{nt} to 5×10^{-17} cm^2/5×10^{-18} cm^2, which implies the lowering of the bulk recombination, increases the FF considerably, and then the conversion

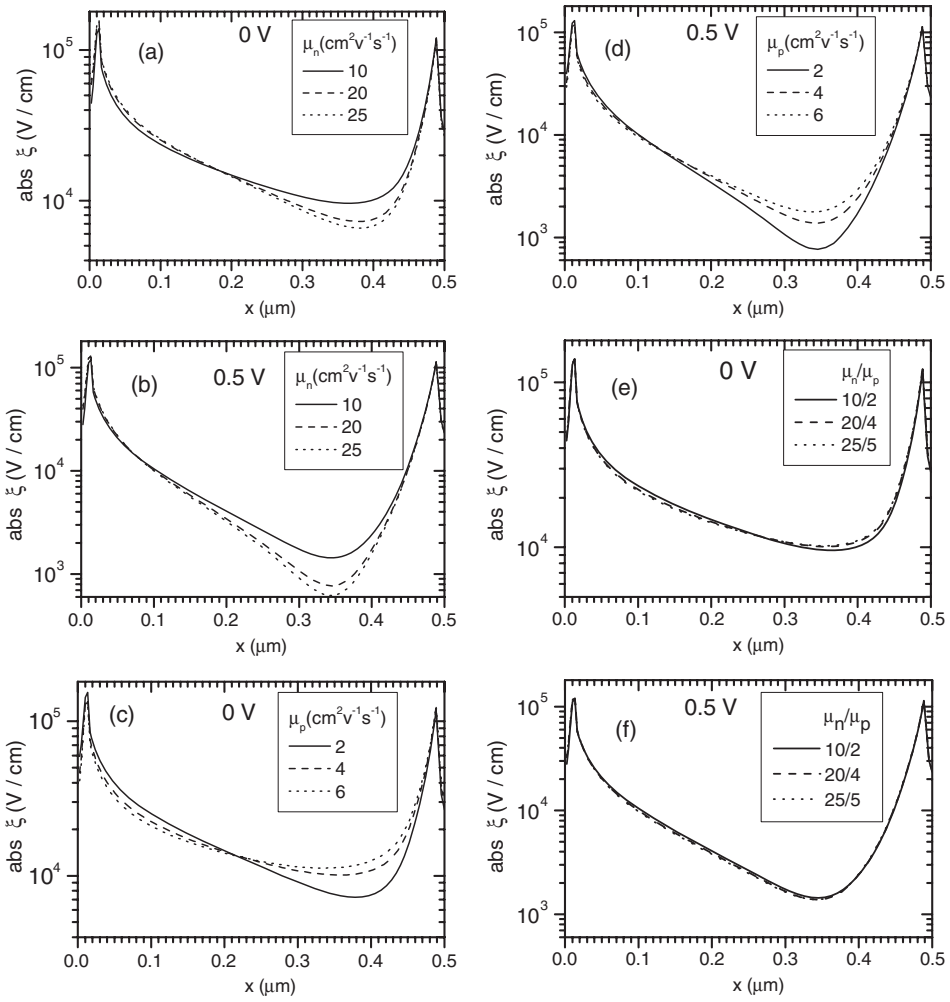

Figure 5. Electrical field versus position (a) at 0 V when μ_p is fixed to 2 cm^2 V^{-1} s^{-1}, (b) at 0.5 V when μ_p is fixed to 2 cm^2 V^{-1} s^{-1}, (c) at 0 V when μ_n is fixed to 20 cm^2 V^{-1} s^{-1}, (d) at 0.5 V when μ_n is fixed to 20 cm^2 V^{-1} s^{-1}, (e) at 0 V when the μ_n/μ_p ratio is fixed to 5, and (f) at 0.5 V when the μ_n/μ_p ratio is fixed to 5.

Table 7. Effect of the capture cross section increase, for the band tail's states, on the output photo-parameters of the solar cell.

$\sigma_{cd}/\sigma_{nd} = 5 \times 10^{-15}/5 \times 10^{-16}$ $\sigma_{ct}/\sigma_{nt} =$	J_{sc} (mA cm^{-2})	V_{oc} (V)	FF	η (%)
$5 \times 10^{-15}/5 \times 10^{-16}$	14.568	0.822	0.65	7.784
$1 \times 10^{-14}/1 \times 10^{-15}$	14.492	0.818	0.619	7.337
$5 \times 10^{-14}/5 \times 10^{-15}$	13.96	0.805	0.545	6.125
	ΔJ_{sc} (%)	ΔV_{oc} (%)	ΔFF (%)	$\Delta\eta$ (%)
	−4.17	−2	−16.15	−21.31

efficiency of the solar cell improves by about 10.6%. However, J_{sc}, shows a slight increase as σ_{ct}/σ_{nt} drops below 5×10^{-16} cm^2/5×10^{-17} cm^2, while V_{oc} remains practically constant.

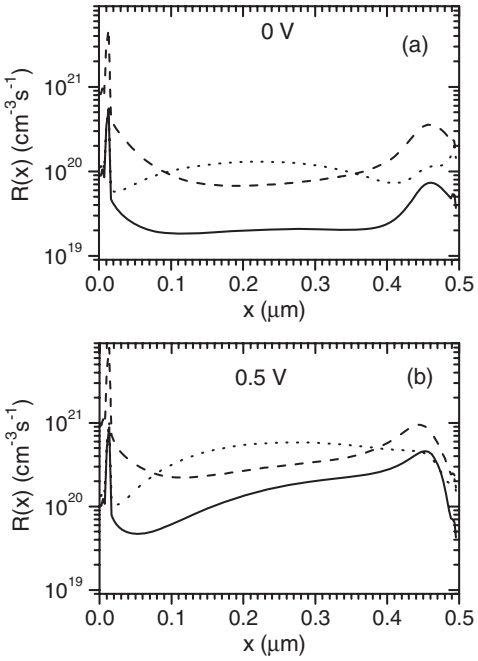

Figure 6. Effect of the capture cross sections on recombination rate versus position, (——) $\sigma_{cd}/\sigma_{nd} = \sigma_{ct}/\sigma_{nt} = 5 \times 10^{-15}/5 \times 10^{-16}$ (cm^2); (- - - -) $\sigma_{cd}/\sigma_{nd} = 5 \times 10^{-14}/5 \times 10^{-15}$ (cm^2), $\sigma_{ct}/\sigma_{nt} = 5 \times 10^{-15}/5 \times 10^{-16}$ (cm^2); (· · · · · ·) $\sigma_{ct}/\sigma_{nt} = 5 \times 10^{-14}/5 \times 10^{-15}$ (cm^2), $\sigma_{cd}/\sigma_{nd} = 5 \times 10^{-15}/5 \times 10^{-16}$ (cm^2); (a) at 0 V and (b) at 0.5 V.

Table 8. Effect of the capture cross section increase, for the dangling bond states, on the output photo-parameters of the solar cell.

$\sigma_{ct}/\sigma_{nt} = 5 \times 10^{-15}/5 \times 10^{-16}$ $\sigma_{cd}/\sigma_{nd} =$	J_{sc} (mA cm^{-2})	V_{oc} (V)	FF	η (%)
$5 \times 10^{-15}/5 \times 10^{-16}$	14.568	0.822	0.65	7.784
$1 \times 10^{-14}/1 \times 10^{-15}$	14.4	0.814	0.632	7.4
$5 \times 10^{-14}/5 \times 10^{-15}$	13.36	0.78	0.566	5.9
	ΔJ_{sc} (%)	ΔV_{oc} (%)	ΔFF (%)	$\Delta\eta$ (%)
	−8.3	−5.1	−12.92	−24.2

Table 9. Effect of the capture cross section decrease, for the band tail's states, on the output photo-parameters of the solar cell.

$\sigma_{cd}/\sigma_{nd} = 5 \times 10^{-15}/5 \times 10^{-16}$ $\sigma_{ct}/\sigma_{nt} =$	J_{sc} (mA cm^{-2})	V_{oc} (V)	FF	η (%)
$5 \times 10^{-15}/5 \times 10^{-16}$	14.568	0.822	0.65	7.784
$5 \times 10^{-16}/5 \times 10^{-17}$	14.637	0.83	0.699	8.49
$5 \times 10^{-17}/5 \times 10^{-18}$	14.645	0.83	0.707	8.6
$10^{-17}/10^{-18}$	14.645	0.83	0.708	8.61

Moreover, there is no further improvement of the output photo-parameters of the solar cell when σ_{ct}/σ_{nt} takes values lower than 5×10^{-17} cm^2/5×10^{-18} cm^2. Ultimately, it seems that

Table 10. Effect of the i-layer DOS increase on the output photo-parameters of the solar cell when $\mu_n/\mu_p = 20/2$ ($cm^2\ V^{-1}\ s^{-1}$).

$\mu_n/\mu_p = 20/2$ i-layer DOS (cm^{-3})	J_{sc} (mA cm^{-2})	V_{oc} (V)	FF	η (%)
5×10^{15}	14.187	0.821	0.58	6.75
1×10^{16}	13.70	0.834	0.5645	6.45
1×10^{17}	9.6	0.842	0.53	4.28
	ΔJ_{sc} (%)	ΔV_{oc} (%)	ΔFF (%)	$\Delta\eta$ (%)
	−32.33	+2.5	−8.62	−36.6

Table 11. Effect of the i-layer DOS increase on the output photo-parameters of the solar cell when $\mu_n/\mu_p = 25/6$ ($cm^2\ V^{-1}\ s^{-1}$).

$\mu_n/\mu_p = 25/6$ i-layer DOS (cm^{-3})	J_{sc} (mA cm^{-2})	V_{oc} (V)	FF	η (%)
5×10^{15}	14.568	0.822	0.65	7.784
1×10^{16}	14.27	0.834	0.627	7.468
1×10^{17}	10.947	0.842	0.565	5.2
	ΔJ_{sc} (%)	ΔV_{oc} (%)	ΔFF (%)	$\Delta\eta$ (%)
	−24.85	+2.43	−13.12	−33.16

J_{sc}, V_{oc} and η are more sensitive to the interface recombination while the FF is more sensitive to the bulk recombination.

3.3. The i-layer DOS effect on the cell output photo-parameters

The i-layer DOS is raised from 5×10^{15} cm^{-3} to 1×10^{17} cm^{-3} when σ_{cd} and σ_{nd} are taken to be 5×10^{-15} cm^2 and 5×10^{-16} cm^2, respectively. The same values are taken for σ_{ct} and σ_{nt}. As indicated in tables 10 and 11, the increase of the i-layer DOS above 10^{16} cm^{-3} considerably degrades the solar cell output parameters, except V_{oc}, although there are some improvements when $\mu_n = 25$ $cm^2\ V^{-1}\ s^{-1}$ and $\mu_p = 6$ $cm^2\ V^{-1}\ s^{-1}$. This can be explained by the fact that when the i-layer DOS is lower than 10^{16} cm^{-3}, the bulk recombination is mainly controlled by recombination via the valence band tail, as shown in figure 7(a), while for an i-layer DOS greater than 10^{16} cm^{-3}, the bulk recombination rate becomes controlled by the density of the dangling bonds (see figure 7(b)), and any further increase considerably deteriorates the solar cell performance. We would like to note here that a similar result has been reported in [12]. As indicated above, V_{oc} increases by only 2.43–2.5% with the increase of the i-layer DOS. A similar observation has been made in [22]; the authors attributed this to the following factors: the properties of the intrinsic layer, the stability of the p/i interface, the change in the ratio between interface and bulk recombination, and the activation of boron atoms in the p layer. Since, in the actual study, no changes for the p/i interface or p layer are considered, the increase of V_{oc} can be attributed to only the third point.

4. Conclusion

A simulation program previously developed by our group for the a-Si:H-based p–i–n solar cell has been used in this paper to investigate the sensitivity of the cell output photo-parameters to

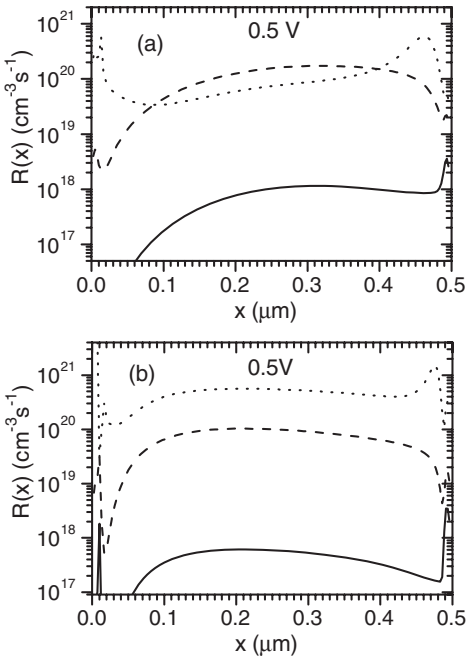

Figure 7. Recombination rate versus position: (——) via the conduction band tail, (- - - -) via the valence band tail, (· · · · · ·) via dangling bonds: (a) when the i-layer DOS $= 10^{16}$ cm^{-3} and (b) when the i-layer DOS $= 10^{17}$ cm^{-3}.

the free carrier's mobilities, the capture cross sections of the gap states and the i-layer DOS. The corroboration of the proposed model has been verified by the fairly good agreement between the calculated output photo-parameters and spectral response compared with experimental measurements carried out by other groups. The salient features obtained from this study are as follows:

- The low values generally attributed to μ_p in the literature make it more important than μ_n in controlling the recombination rate near the interface regions as well as in the bulk of the device. Then μ_p plays a crucial role in the improvement or the deterioration of the cell performance, a result which was previously confirmed by other groups. Moreover, by keeping the μ_n/μ_p ratio constant while both μ_n and μ_p are raised, no change is observed in the electrical field versus position. This means that the electrical field depends on the μ_n/μ_p ratio instead of μ_n or μ_p separately.
- By changing, independently, the capture cross sections of the band's tails and that of dangling bonds, we found that the recombination rate near the interface regions is more sensitive to σ_{cd} and σ_{nd}, while in the bulk it is more sensitive to σ_{ct} and σ_{nt}. The last observation is, obviously, conditioned by the fact that the tail state density must exceed that of dangling bonds. In addition, it seems that J_{sc}, V_{oc} and η are more affected by recombination at the interface regions than that in the bulk, contrarily to the FF.
- Finally, the output photo-parameters' degradation owing to the i-layer DOS increase is more noticeable when the latter governs the bulk recombination instead of the valence band tail state's density. This condition is fulfilled as the i-layer DOS becomes greater than 10^{16} cm^{-3}.

References

[1] Moon B Y, Choi J H, Kim J G, Jang J, Kim D W, Bae S S and Yoon K S 1997 *Sol. Energy Mater. Sol. Cells* **49** 113
[2] Meftah A M, Meftah A F, Hiouani F and Merazga A 2004 *J. Phys.: Condens. Matter* **16** 2003
[3] Meftah A M, Meftah A F and Merazga A 2006 *J. Phys.: Condens. Matter* **18** 5459
[4] Kurata M 1982 *Numerical Analysis for Semiconductor Devices* (Lexington, MA: Heath)
[5] Selberherr S 1984 *Analysis and Simulation of Semiconductor Devices* (Berlin: Springer)
[6] Mott N F 1970 *Phil. Mag.* **22** 7
[7] Street R A 1991 *Hydrogenated Amorphous Silicon* ed R A Street (Cambridge: Cambridge University Press)
[8] Tasaki H, Kim W Y, Hallerdt M, Konagai M and Takahashi K 1988 *J. Appl. Phys.* **63** 550
[9] Mittiga A, Fiorini P, Falconieri M and Evangelisti F 1989 *J. Appl. Phys.* **66** 2667
[10] Tchakarov S, Roca i Cabarrocas P, Dutta U, Chatterjee P and Equer B 2003 *J. Appl. Phys.* **94** 7317
[11] Poissant Y, Chatterjee P and Roca i Cabarrocas P 2003 *J. Appl. Phys.* **94** 7305
[12] Chatterjee P 1994 *J. Appl. Phys.* **76** 1301
[13] Powell M J and Deane S C 1996 *Phys. Rev.* B **53** 10121
[14] Stiebig H, Siebke F, Beyer W, Beneking C, Rech B and Wagner H 1997 *Sol. Energy Mater. Sol. Cells* **48** 351
[15] de Seta M, Fiorini P, Evangelisti F and Armigliato A 1989 *Superlatt. Microstruct.* **5** 149
[16] Asano A, Ichimura T, Uchida Y and Sakai H 1988 *J. Appl. Phys.* **63** 2346
[17] Murthy R V R, Dutta V and Singh S P 1994 *J. Appl. Phys.* **33** L1581
[18] Dutta V and Murthy R V R 1997 *J. Appl. Phys.* **36** 6687
[19] Schubert M B 1999 *Thin Solid Films* **337** 240
[20] Martins R, Aguas H, Ferreira I, Fortunato E and Guimaraes L 2000 *Solar Energy* **69** (Suppl.) 257
[21] Hack M and Shur M 1985 *J. Appl. Phys.* **58** 997
[22] Poissant Y and Roca i Cabarrocas P 2000 *J. Non-Cryst. Solids* **266–269** 1134